Near-Field Coherent Spectroscopy and Microscopy of a Quantum Dot System

J. R. Guest,[1] T. H. Stievater,[1] Gang Chen,[1] E. A. Tabak,[1] B. G. Orr,[1] D. G. Steel,[1]* D. Gammon,[2] D. S. Katzer[2]

We combined coherent nonlinear optical spectroscopy with nano–electron volt energy resolution and low-temperature near-field microscopy with subwavelength resolution ($<\lambda/2$) to provide direct and local access to the excitonic dipole in a semiconductor nanostructure quantum system. Our technique allows the ability to address, excite, and probe single eigenstates of solid-state quantum systems with spectral and spatial selectivity while simultaneously providing a measurement of all the various time scales of the excitation including state relaxation and decoherence rates. In analogy to scanning tunneling microscopy measurements, we can now map the optical local density of states of a disordered nanostructure. These measurements lay the groundwork for studying and exploiting spatial and temporal coherence in the nanoscopic regime of solid-state systems.

The study of fundamental physics and the development of nanotechnologies continue to drive nanostructures to smaller length scales, resulting in advances in material preparation techniques and the outgrowth of diagnostic and control capabilities. Optical interactions with many of these systems are of critical importance because optical spectroscopy has evolved extensively in recent years to provide insight into their electronic structure and dynamics. Moreover, in many cases, coherent optical control and optical manipulation play a fundamental role in the functioning of some proposed devices.

To explore and address these systems on nanometer-length scales, traditional far-field optical techniques fall short because they are limited to resolution on a length scale of $\lambda/2$ under the best conditions. By sacrificing the ability to image, samples with apertures (*1*) or with etched mesa structures (*2*) have reduced the number of nanostructures in the field of view to a small number. By probing these samples with conventional optical spectroscopies, the ensemble averaging that occurs in typical far-field measurements is eliminated because each nanostructure, characterized by a seemingly random but unique energy level structure, is now spectrally resolved. The pioneering work of near-field scanning optical microscopy (*3*) has demonstrated the feasibility of obtaining images of electronic structures far beyond the classical limit by probing a system through a small aperture at the end of a scanning probe.

[1]Harrison M. Randall Laboratory of Physics, The University of Michigan, Ann Arbor, MI 48109, USA. [2]The Naval Research Laboratory, Washington DC 20375, USA.

*To whom correspondence should be addressed. E-mail: dst@umich.edu

Anticipation of rapid growth in this field has led to the proposal of quantum mechanical devices that require direct access to eigenstates with spectral and spatial selectivity (*4*). The current embodiment of these methodologies, however, either relies on the indirect optical probe of photoluminescence (PL), which requires spectral and often spatial diffusion for detection, or sacrifices spatial information by probing the system through fixed apertures.

We present a technique that combines the direct optical probe and spectral selectivity of coherent nonlinear optical spectroscopy with the spatial selectivity of near-field microscopy at low temperature, allowing us the ability to excite and probe the same quantum transition in an extended structure with subwavelength resolution. This capability provides a means to map the optical dipole in space and energy with high resolution, revealing the optical local density of states (LDOS) of the system in analogy to previous scanning tunneling microscopy (STM) work (*5*) that mapped out the electronic LDOS. In addition to affording neV energy resolution, this methodology also provides dynamical information on the time evolution of the eigenstate. The work builds on previous low-temperature transient nonlinear measurements at high spatial resolution (*6*, *7*) and opens the door to comparison with theoretical work on the local optical properties of nanoscopic semiconductor systems (*8*–*11*).

In this integrated approach (Fig. 1A), the near-field microscope was operated at 4 K to reduce phonon-induced broadening and perform high-resolution spectroscopy on these exciton systems. The near-field probe, etched and coated with 100 nm of aluminum, was brought into the vicinity of the sample (<10 nm) and maintained there by feeding back on a shear force signal obtained through a phase-sensitive piezo-microphone technique (*12*). The optical fields were delivered to the sample collinearly polarized and at similar amplitudes. The transmitted fields were detected by a built-in photodiode or collected by optics and delivered to a room-temperature avalanche photodiode (APD). The signal of interest was recovered through phase-sensitive detection at the modulation difference frequency (20 kHz) of the optical beams provided by two frequency-locked continuous-wave (CW) tunable lasers (linewidths ~ neV) (*13*, *14*). Two interferometers were used to verify the calibration and orthogonality of spatial axes at 4 K.

The nanostructure investigated in this work was grown by molecular beam epitaxy and consists of a 62 Å layer of GaAs sandwiched between two 250 Å layers of $Al_{0.3}Ga_{0.7}As$. The

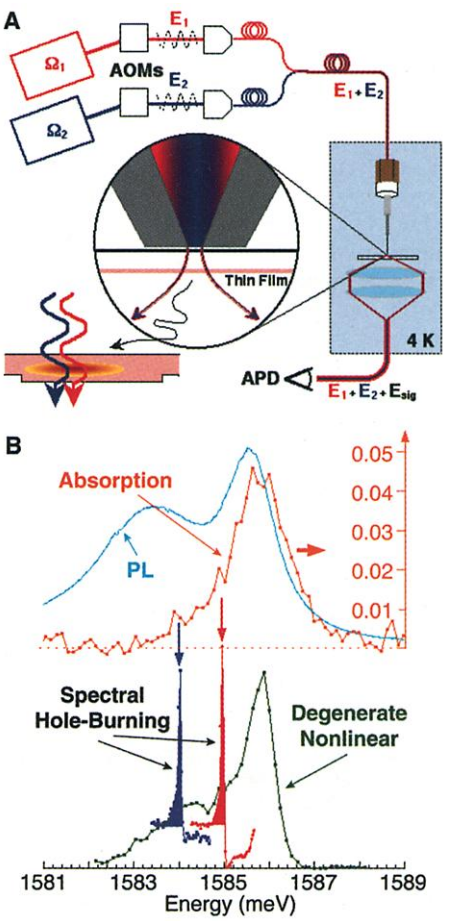

Fig. 1. (**A**) Schematic of the experimental setup. Two frequency-stabilized lasers are acousto-optically modulated (AOM) at (slightly different) high frequencies (~100 MHz) and coupled into the same near-field probe, which is maintained near the sample surface at 4 K. The transmitted fields are recollected and transmitted through an optical fiber to an APD. (**B**) Far-field ensemble studies. Absorption, PL, degenerate nonlinear, and spectral hole-burning spectra are shown. The energies of the pump fields for the spectral hole-burning studies are indicated by the arrows.

growth of the structure was interrupted for 2 min at the interfaces in order to increase the length scale of the disorder and lead to the formation of interface quantum dots (*1*, *15*). The sample was mounted on a sapphire disk (*c* axis normal) with the "lift-off" technique (*16*) to remove the substrate for transmission and preserve scanning probe access to the quantum wells. The disordered layer was buried 130 nm in the sample to prevent surface broadening of the spectral lines; however, this led to a spatial resolution that was degraded relative to that available within a few tens of nm of the probe. This was partially compensated by the nonlinearity of our signal mechanism, which enhanced the achievable spatial resolution (*17*).

We first show far-field ensemble measurements based on both luminescence/absorption and coherent nonlinear optical spectroscopy (Fig. 1B). The luminescence curve (light blue) shows high- and low-energy peaks that are due to excitons localized in the 22- and 23-monolayer-wide regions of the quantum well, respectively; this bimodal distribution of confinement energies arises directly from the growth interruptions (*1*). The linear absorption (orange) superimposed on the luminescence from the single layer reveals the usual Stokes shift associated with highly disordered systems. As expected, the degenerate ($\Omega_1 = \Omega_2$) nonlinear response (green) largely coincides with the absorption. Furthermore, the absence of zero crossings in the degenerate nonlinear line shape demonstrates that the nonlinear optical response is dominated by saturation with no detectable contributions from other many-body effects as seen in higher dimensional systems. Superimposed on this curve is the nondegenerate ($\Omega_1 \neq \Omega_2$) nonlinear response (red and blue) for two different pump-field wavelengths (shown by the arrows). These systems show spectral hole-burning by the pump field (*18*) and, in contrast to higher dimensional systems (*19*, *20*), an absence of spectral diffusion. The linewidth can therefore be characterized by $\approx 4\hbar\gamma$, where $\hbar$ is Planck's constant divided by 2π and γ is the dephasing rate; in Fig. 1B, $\hbar\gamma \cong 17$ μeV (in the language of nuclear magnetic resonance, $T_2 \equiv 1/\gamma \cong 39$ ps).

The direct, coherent, and local nature of the nonlinear measurement through the microscope can be understood by examining the spatially dependent third-order polarization induced by the two independent optical fields. As the spatial resolution in our experiment does not approach the excitonic Bohr radius in GaAs (~10 nm), a local description of the optically induced polarization is sufficient (*21*). Our measurements are sensitive to

$$P^{(3)}_{NL}(\boldsymbol{r},\Omega_1,\Omega_2) \propto \chi^{(3)}(\boldsymbol{r},\Omega_s=\Omega_2-\Omega_1+\Omega_1) E_1(\boldsymbol{r},\Omega_1) E_1^*(\boldsymbol{r},\Omega_1) E_2(\boldsymbol{r},\Omega_2) \quad (1)$$

where $\chi^{(3)}$ is the resonant nonlinear susceptibility, $\boldsymbol{r}$ is the spatial position in the plane of the thin film, and Ω_i is the optical frequency of the field i. The optical field generated by the imaginary part of this polarization at the frequency $\Omega_S = \Omega_2$ is homodyne detected with the transmitted probe beam E_2^*. The signal $S_{NL} \propto E_2^* \mathrm{Im}\{P_{NL}^{(3)}\}$ is then a function of energy and position. The optical field in the plane of the thin film can be written as $E_i(\boldsymbol{r},\Omega_i) = E_i(\Omega_i)\xi(\boldsymbol{r} - \boldsymbol{R})$, where ξ is the spatial profile and $\boldsymbol{R}$ is the near-field probe position. Integrating the response over space convolves the spatial dependence of the excitonic dipole with this optical field profile, resulting in a measured response $S_{NL}(\boldsymbol{R},\Omega_1,\Omega_2)$. This is a complete formulation of the response in our regime (*21*), showing that $\chi^{(3)}$ can be used as a direct local probe of the distributed optical dipole in our system.

In a mapping (Fig. 2) of our disordered system with the fully degenerate ($\Omega_1 = \Omega_2 = \Omega$) nonlinear optical response [$S_{NL}(\boldsymbol{R},\Omega) \equiv S_{NL}(\boldsymbol{R},\Omega,\Omega)$] of the optically active states in a 2-μm by 2-μm by 7.44-meV region, the data display discrete excitonic resonances that have been isolated from the inhomogeneous response shown in the far-field ensemble measurement (Fig. 1B). The measurements show that the excitonic resonances are localized in space. The nonlinear data, although visually appearing similar to the PL data in (*3*), are substantially different as evidenced by detailed analysis. In the wings of the inhomogeneous distribution, the predominantly positive signal is indicative of a saturation-dominated response, showing that these localized states display an atom-like character that is profoundly different from that in higher dimensional systems. However, near 1586 meV, the response of specific resonances includes a negative component (i.e., induced absorption) and is associated with line shifts and broadening, suggesting that the excitonic response in the region is far less localized and exhibits features associated

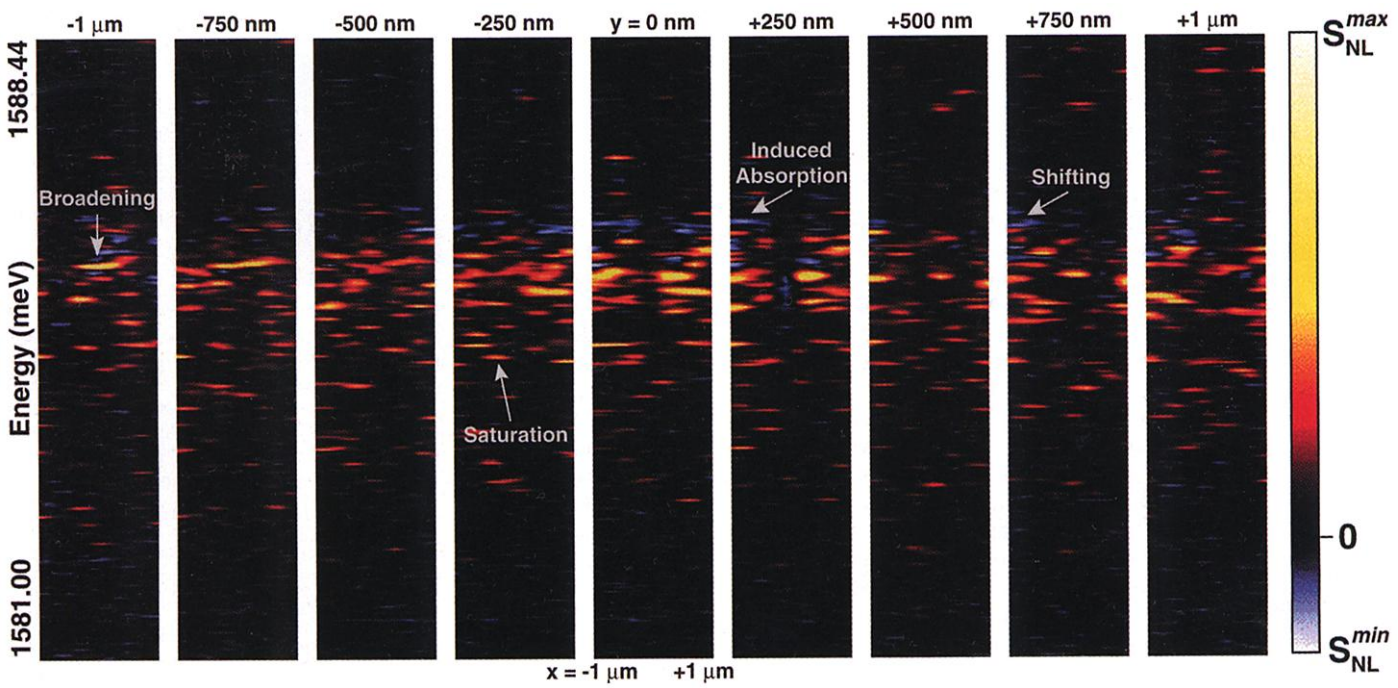

Fig. 2. Three-dimensional CW nonlinear response of the excitonic dipole in a data set spanning 2 μm by 2 μm by 7.44 meV. The vertical axis is energy, the horizontal axis is x, and each two-dimensional slice of data is taken at a different y value. Positive signal, or saturation, is indicated by red to white. Negative signal is indicated by blue. Signatures of saturation, shifting, broadening, and induced absorption are annotated.

with many-body interactions. That these features can be seen at the same energy suggests the coexistence of strongly and weakly localized states at different spatial locations as predicted by Zimmerman and co-workers (*22*) and inferred from a decay-associated spectral analysis of far-field photon echo data in our laboratory (*23*). Even more distinct from the PL data in (*3*) is the appearance of isolated fully negative signals showing resonances characterized (in the nonlinear optical response) by induced absorption, indicating the observation of the biexciton (*18, 24*).

This spectral and spatial mapping of the optically active eigenstates of the system is a nonlinear mapping of the optical LDOS. In addition to providing a valuable diagnostic for this nanostructure system, this mapping also provides the critical experimental connection to the quantum mechanical description of the system. A similar connection has previously been made in a very different experimental regime; through STM methodologies, Crommie *et al.* were able to map the LDOS of surface electronic states on copper (*5*). Although these tunneling measurements offer unparalleled spatial resolution, they are limited by poor spectral resolution, are restricted to the study of short-lived surface states, and are intrinsically incoherent. In contrast, the direct optical spectral and spatial mapping of the excitonic dipole through CW nonlinear near-field spectroscopy and microscopy sacrifices the spatial resolution available to STM in exchange for unmatched spectral resolution (<10 neV), access to stable buried individual nanostructures, the ability to induce and detect electronic coherences, and a window on the energy relaxation and dephasing dynamics of the excitation. Statistical analysis of the optical LDOS has the potential to reveal the underlying framework for this quantum system; evidence for energy-level repulsion (*25, 26*), for example, has already been revealed in our system (*27*). In addition, by studying optically accessible excitons in semiconductor nanostructures, we are exploring systems of considerable general interest and laying the foundation for addressing, preparing, and controlling these systems coherently.

The nonlinear mapping of the optical LDOS characterizes many isolated eigenstates and is separable in energy and space:

$$S_{NL}(\boldsymbol{R},\Omega) = \sum_n \zeta_n f_n(\Omega) h_n(\boldsymbol{R}) \qquad (2)$$

where, for a localized excitonic eigenstate $|n\rangle$, ζ_n is a constant, $f_n(\Omega)$ is the line shape of the nonlinear response, and $h_n(\boldsymbol{R})$ is a nonlinear function of the optical-field distribution and the excitonic wave function (*21*). The concept of the optical LDOS is exemplified in Fig. 3A, where a three-dimensional data set spanning 2 μm by 2 μm but only 100 μeV in energy is represented by a series of images taken at different energies. For these isolated homogeneously broadened resonances, the spectral line shapes take the form of a Lorentzian squared where the Lorentzian linewidth (full width at half-maximum) is $2\hbar\gamma_n$. As seen in Fig. 3B, the data are well fit by this form and reveal an $\hbar\gamma_n$ that ranges from 17 to 29 μeV ($T_2 \equiv 1/\gamma_n \approx$ 23 to 30 ps) in strong agreement with the far-field values obtained from hole-burning (Fig. 1B) and with those obtained from studies through apertures (*13*). Unlike PL spectra, which frequently have instrument-limited linewidths for these systems, the high resolution of the frequency-stabilized lasers provides an unambiguous result.

Although the spatial mapping $h_n(\boldsymbol{R})$ of the resonances in Fig. 3A largely reflects the instrument response of the near-field probe, we observed indications of structure beyond our spatial resolution. A lower energy eigenstate (1583.120 meV), which is well represented by a single Lorentzian squared (*28*), is imaged in Fig. 3C. Interferometrically calibrated line scans along the crystal axes as compared with the instrument reponse (Fig. 3D) show unambiguously that this resonance is elongated along the [$\bar{1}$10] axis by ~200 nm. This length scale and direction of elongation coincide with the previously reported properties of the (larger) monolayer islands that form the quantum dots (*1*). Taken together with the direct nature of the nonlinear measurement (i.e., no spatial diffusion), these factors suggest that we are observing indications of the center-of-mass wave function through our nonlinear near-field technique.

The various time scales associated with the decoherence and energy relaxation of the optically induced quantum coherence can be extracted by using the full power of coherent nonlinear spectroscopy. The nonlinear optical response of quantum dot excitons is composed of an incoherent and a coherent contribution. The incoherent contribution is due to simple phase-insensitive saturation of the optical resonance by one optical field that is then probed by the second optical field, whereas the coherent contribution arises from the mixing of the two fields through the excitation and is highly sensitive to their relative phase. In the above degenerate nonlinear data sets, these contributions are indistinguishable, and, as a result, only the overall dephasing rate is accessible. To differentiate between these contributions (and between the various time scales, as discussed below), we used two nondegenerate ($\Omega_1 \neq \Omega_2$) optical fields that have a mutual coherence time (~hundreds of nanoseconds) that is much longer than the time scale associated with the evolution of the quantum dot excitation (~tens of picoseconds).

The influence of the coherent contribution is seen in the nondegenerate nonlinear optical response shown in Fig. 4. For a two-level system, the spectral component of the nondegenerate nonlinear response from Eq. 2 takes the form derived from a solution of the density matrix equations used to model the quantum dot exciton (*13*):

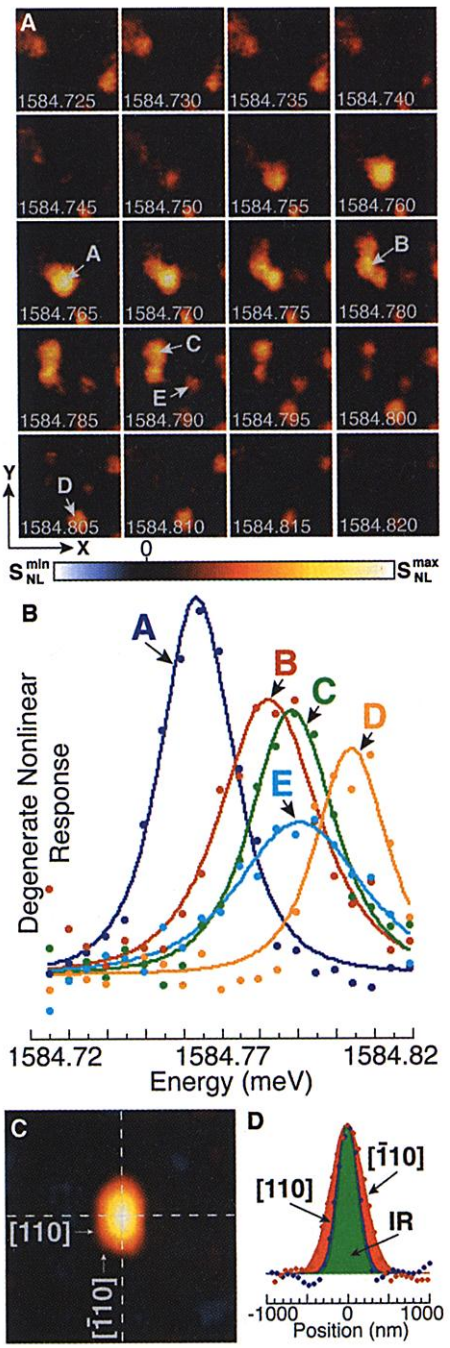

Fig. 3. High spectral resolution three-dimensional CW nonlinear response. (**A**) Three-dimensional CW nonlinear response spanning 2 μm by 2 μm by 100 μeV represented by spatial images recorded at different energies (annotated in meV). (**B**) The spectral line shapes for the five eigenstates labeled in (A) are fit by Lorentzians squared. (**C**) Spatial mapping (2 μm by 2 μm at 1583.120 meV) of an excitation that is larger than the spatial resolution; line cuts through the image along the [$\bar{1}$10] (red) and [110] (blue) crystal axes are compared with the instrument response (green) in (**D**).

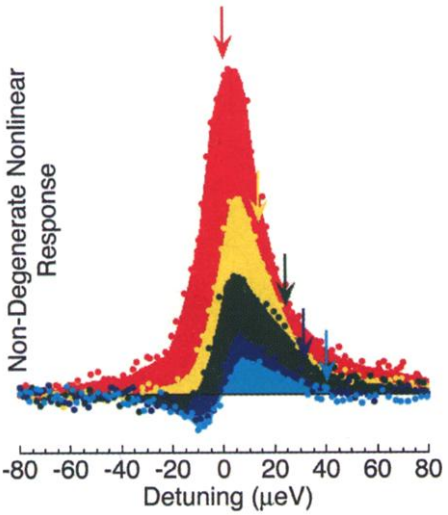

Fig. 4. Nondegenerate ($\Omega_1 \neq \Omega_2$) spectral mapping of a single eigenstate. Each spectrum represents a different spectral position of the pump (Ω_1), which is indicated by the arrow.

$$f_n(\Omega_1,\Omega_2) = \frac{1}{8(\gamma_n + i\Delta_{n2})} \left[\frac{1}{\Gamma_n} \left(\frac{1}{\gamma_n - i\Delta_{n1}} + \frac{1}{\gamma_n + i\Delta_{n1}} \right) + \frac{1}{\Gamma_n + i(\Delta_{n2} - \Delta_{n1})} \left(\frac{1}{\gamma_n - i\Delta_{n1}} + \frac{1}{\gamma_n + i\Delta_{n2}} \right) \right] + c.c. \quad (3)$$

where $\Delta_{ni} = \omega_n - \Omega_i$ and indices 1 and 2 refer to the pump and probe fields, respectively (*29*). As discussed in (*13*), the line shape is distinctive in two limits. In the limit where excitation decoherence rate ($T_2^{-1} = \gamma_n$) greatly exceeds the energy relaxation rate ($T_2^{-1} = \Gamma_n$), the line shape is characterized by a simple Lorentzian resembling a spectral hole with width $2\hbar T_1^{-1}$ centered at the pump frequency superimposed on a much broader Lorentzian with width $2\hbar T_2^{-1}$ centered at the quantum dot exciton resonance. In the limit where the only decoherence is due to energy relaxation (i.e., $T_2^{-1} \approx T_1^{-1}/2$), the line shape transforms markedly to one that arises from interference, resembling dispersion, distinctly differentiating the two limits. The data in Fig. 4 show this interference line shape unambiguously; as the pump field is tuned away from line center, a dispersion-like line shape due to the coherent contribution emerges in the nonlinear response. This is consistent with no substantial pure dephasing, such that $T_2 \cong 25$ ps and $T_1 \equiv 1/\Gamma_n \cong 16 \pm 3$ ps. This lack of extra dephasing allows for the coherent coupling of the optical fields through the eigenstate and the temporal modulation of the excitation of a single exciton [population pulsations (*30*)] at the difference frequency $\Omega_2 - \Omega_1$ (up to ~12 GHz for the eigenstate examined in Fig. 4). The single resonance dephasing rate discussed above is consistent with the ensemble-averaged dephasing rate extracted from Fig. 1B and similar to that reported in (*13*).

Moving beyond the paradigm of single exciton spectroscopy, the optical LDOS has been obtained for a quantum dot system. At the single eigenstate level, our two optical fields are coherently coupled through the excitonic resonance, allowing us to determine the various time scales associated with the excitation. These experiments have laid the foundation for selectively addressing and controlling individual eigenstates in a coherent manner through spatial as well as spectral discrimination. This technique is applicable to any optically active system in the vicinity of the sample surface, such as other semiconductor nanostructures or single molecules, making it easily adaptable to the changing frontier of nano-optics and quantum-information technology.

References and Notes

1. D. Gammon, E. S. Snow, B. V. Shanabrook, D. S. Katzer, D. Park, *Phys. Rev. Lett.* **76**, 3005 (1996).
2. S. Fafard, R. Leon, D. Leonard, J. L. Merz, P. M. Petroff, *Phys. Rev. B* **50**, 8086 (1994).
3. H. Hess, E. Betzig, T. D. Harris, L. N. Pfeiffer, K. W. West, *Science* **264**, 1740 (1994).
4. A. Imamoglu *et al.*, *Phys. Rev. Lett.* **83**, 4204 (1999).
5. M. F. Crommie, C. P. Lutz, D. M. Eigler, *Nature* **363**, 524 (1993).
6. J. Levy *et al.*, *Phys. Rev. Lett.* **76**, 1948 (1996).
7. M. Vollmer *et al.*, *Appl. Phys. Lett.* **74**, 1791 (1999).
8. O. Mauritz, G. Goldoni, F. Rossi, E. Molinari, *Phys. Rev. Lett.* **82**, 847 (1999).
9. S. Savasta, G. Martino, R. Girlanda, *Phys. Rev. B.* **61**, 13852 (2000).
10. B. Hanewinkel, A. Knorr, P. Thomas, S. W. Koch, *Phys. Rev. B* **55**, 13715 (1997).
11. G. W. Bryant, *Appl. Phys. Lett.* **72**, 768 (1998).
12. J. Barenz, O. Hollricher, O. Marti, *Rev. Sci. Instrum.* **67**, 1912 (1995).
13. N. H. Bonadeo *et al.*, *Phys. Rev. Lett.* **81**, 2759 (1998).
14. G. Chen *et al.*, *Science* **289**, 1906 (2000).
15. Q. Wu, R. D. Grober, D. Gammon, D. S. Katzer, *Phys. Rev. Lett.* **83**, 2652 (1999).
16. E. Yablonovich, T. Gmitter, J. P. Harbison, R. Bhat, *Appl. Phys. Lett.* **51**, 2222 (1987).
17. M. K. Lewis, P. Wolanin, A. Gafni, D. G. Steel, *Opt. Lett.* **23**, 1111 (1998).
18. G. Chen *et al.*, unpublished data.
19. J. T. Remillard *et al.*, *Phys. Rev. Lett.* **62**, 2861 (1989).
20. H. Wang, M. Jiang, D. G. Steel, *Phys. Rev. Lett.* **65**, 1255 (1990).
21. The simple theoretical treatment of the nano-optical response described herein is adequate only in the limit that the spatial resolution comfortably exceeds the length scale that characterizes Coulomb correlations, i.e., the excitonic Bohr radius. Below this limit, a new regime is entered in which the nonlocal character of the light-matter interaction and Coulomb correlation effects dominate the local optical response; a nonlocal formulation must then be used [see (*8*, *9*)].
22. U. Jahn *et al.*, *Phys. Rev. B* **56**, R4387 (1997).
23. J. Erland *et al.*, *Phys. Rev. B* **60**, R8497 (1999).
24. T. Takagahara, *Phys. Rev. B* **39**, 10206 (1989).
25. E. Runge, R. Zimmermann, *Phys. Stat. Sol. b* **206**, 167 (1998).
26. F. Intonti *et al.*, *Phys. Rev. Lett.* **87**, 076801 (2001).
27. J. R. Guest *et al.*, paper presented at Nonlinear Near-Field Spectroscopy and Microscopy of Single Excitons in a Disordered Quantum Well, QELS, 2000.
28. J. R. Guest *et al.*, data not shown.
29. In our geometry, each field serves as both the pump and probe.
30. P. Meystre, M. Sargent, *Elements of Quantum Optics* (Springer-Verlag, New York, ed. 2, 1991).

31. This work was supported in part by the Office of Naval Research, the National Security Agency, and Advanced Research and Development Activity under Army Research Office contract number DAAG55-98-1-0373, the Air Force Office of Scientific Research under grant number F49620-99-1-0045, the NSF under grant DMR 0099572, and DARPA/Spins. One of the investigators (D.G.S.) thanks the Guggenheim Foundation for their support.

22 June 2001; accepted 15 August 2001

Hydrogen Sensors and Switches from Electrodeposited Palladium Mesowire Arrays

Frédéric Favier,[1] Erich C. Walter,[2] Michael P. Zach,[2] Thorsten Benter,[2] Reginald M. Penner[2]*

Hydrogen sensors and hydrogen-activated switches were fabricated from arrays of mesoscopic palladium wires. These palladium "mesowire" arrays were prepared by electrodeposition onto graphite surfaces and were transferred onto a cyanoacrylate film. Exposure to hydrogen gas caused a rapid (less than 75 milliseconds) reversible decrease in the resistance of the array that correlated with the hydrogen concentration over a range from 2 to 10%. The sensor response appears to involve the closing of nanoscopic gaps or "break junctions" in wires caused by the dilation of palladium grains undergoing hydrogen absorption. Wire arrays in which all wires possessed nanoscopic gaps reverted to open circuits in the absence of hydrogen gas.

Chemical sensors based on nanowires usually operate through a change in resistance induced by the surface adsorption of analyte molecules. Tao and co-workers (*1*) have demonstrated that the conductivity of gold nanowires changes upon exposure to mole-